Out of plane loading of drag embedment anchors for floating renewable energy technologies

Davidson, Craig; Brennan, Andrew; Brown, Michael; Inglis, Lloyd; Vasudevan, Sojan

Publication date:
2023

Davidson, C, Brennan, A, Brown, M, Inglis, L & Vasudevan, S 2023, 'Out of plane loading of drag embedment anchors for floating renewable energy technologies', Paper presented at 9th International SUT OSIG Conference "Innovative Geotechnologies for Energy Transition", London, United Kingdom, 12/09/23 - 14/09/23 pp. 1241-1248.https://www.eventsforce.net/sut/frontend/reg/thome.csp?pageID=264&ef_sel_menu=5&eventID=2

Out of plane loading of drag embedment anchors for floating renewable energy technologies

C. Davidson, A. Brennan & M. Brown
University of Dundee, Dundee, UK

L. Inglis
Bruce Anchor, Aberdeen, UK

S. Vasudevan
InterMoor, Aberdeen, UK

ABSTRACT: Drag embedment anchors are a technology that has developed through many years' experience. However, as demand increases for anchoring of clean energy technologies offshore, so the requirements of modern drag embedment anchors have evolved. A more resilient infrastructure requires improved understanding of how an anchor will perform in abnormal loading conditions, such as when a load is applied out of plane to the direction in which it was installed. This work presents data from a set of tests carried out on the University of Dundee geotechnical centrifuge in order to understand how a typical 12t Bruce GP drag embedment anchor performs in sandy soil. Initial tests in loose and medium-dense soil conditions identify the ultimate holding capacity (UHC) of the anchor. Subsequent tests were then conducted in which the anchors were dragged to 60% of the UHC, to mimic current installation practice, before being loaded to failure at angles of 20, 30 and 45°, inclined to the in-line direction. Measurements of the out-of-plane holding capacity were compared to the in-line loading conditions and demonstrated that holding capacities under side-loading angles up to 20° were similar to the straight pull capacity.

1 **Introduction**

Historically, floating offshore units, such as those used in the oil & gas industry, have been designed with redundant mooring systems. Redundancy implies that if a mooring line fails, one or more adjacent lines will be available to maintain the unit's orientation and position within acceptable limits. In contrast, for a range of reasons, some of the developers in the floating wind industry are preferring to use non-redundant mooring systems.. A line failure, especially in a 3-line mooring system, is likely to result in large offsets of the platform in the opposite direction to the failed line. This could cause a change in the direction of loading at the anchor point. If drag embedment anchors (DEA) are used, the anchor performance at this new "side-loaded" direction will have to be assessed.

Typically, the use of DEAs has been limited to loading in the mooring line installation direction. Data is therefore limited on their performance under side-load conditions and there is no defined method for verifying the performance in such conditions. This paper presents details of the actuator development and results of centrifuge tests conducted by the University of Dundee in conjunction with Bruce Anchor. The centrifuge testing method enables drag anchor models to be installed and tested at full-scale stress levels and in a range of soil conditions. It can be adapted to benchmark performance of drag anchors based on applied mooring loads, pull directions and site-specific soil conditions.

2 **Centrifuge modelling methodology**

2.1 *Introduction*

Centrifuge modelling methods were selected to investigate the drag embedment anchor performance under side-loading to correctly reproduce effective stress-dependent aspects such as the dilation of granular material during shearing, and the interaction between the model and soil.

This section presents the relevant scaling factors; a description of the actuator and container; preparation properties of the sand bed; details of the data acquisition system and a summary of the test programme.

2.2 *Scaling laws and drainage conditions*

All tests were conducted using the University of Dundee centrifuge at 50g (at the surface of the sand). Fully drained conditions were assumed (i.e., no excess pore pressures) and all tests were com-

pleted using dry sand and scaled as the saturated equivalent. Dry sand testing is significantly faster and more cost effective and has been demonstrated to provide the same results as saturated tests under drained conditions (Li et al., 2010). The scaling factors relevant to this study are presented in Table 1. The length scale was chosen to be 1/80 to maximise lateral movement of the anchor before encountering boundary effects from the container walls. For clarity, all results presented in this paper are in prototype scale unless directly specified.

Table 1. Centrifuge scaling laws to convert between model and prototype scale values (Muir Wood, 2014).

Model parameter	Scaling law	This study
Lengths & displacements	N_L	*1/80*
Acceleration & gravity	N_G	*50*
Mass density	N_ρ	*1.61*
Force	$N_\rho N_G N_L^3$	$1/80^2$
Stress	$N_\rho N_G N_L$	*1*

2.3 *Centrifuge testing equipment*

To accommodate the large displacements required for testing a DEA, a 1.6m long model container and linear actuator was used (Figure 1). This equipment has been previously used for similarly large displacement testing of ploughs and trains (Robinson et al., 2019). The actuator comprises a sled, mounted on low friction rails, driven by a belt/pulley system and a geared DC motor. With the anchor attached, the actuator can travel up to 650mm.

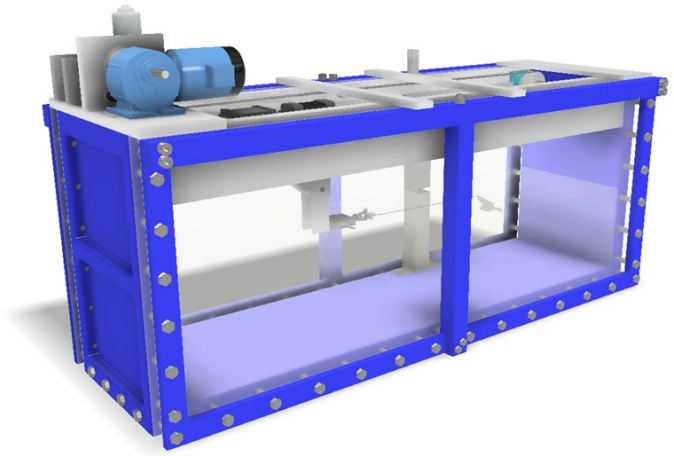

Figure 1. 3D model of centrifuge container and actuator with anchor in-situ (sand shown as transparent for visibility)

For straight pulls of the anchor, the model was attached to the linear actuator with 1.5mm steel wire rope via a 5kN loadcell (Tedea Huntleigh type 616) mounted to an arm below the travelling sled which positioned the loadcell 1mm above the sand surface. A swivel and shackle were located at the loadcell end of the forerunner to minimise potential torsional forces from tensioning of the twisted wire rope. The anchor padeye to loadcell distance was 440mm. This arrangement is illustrated in Figure 2. Displacement of the anchor is not measured directly and is taken as the horizontal distance travelled by the actuator as measured by a draw wire transducer (Multicomp SP1-50).

The out-of-plane anchor load tests were conducted after a straight installation pull of the anchor to a target load of 60% of the ultimate holding capacity (UHC), in the value of which was measured from the equivalent straight pull test. The drag distances required to reach 0.6UHC was larger than the space available between the start of the test and the out-of-plane test equipment, thus the anchor was pre-embedded in one of the side pull tests which would otherwise require too long an installation drag distance.

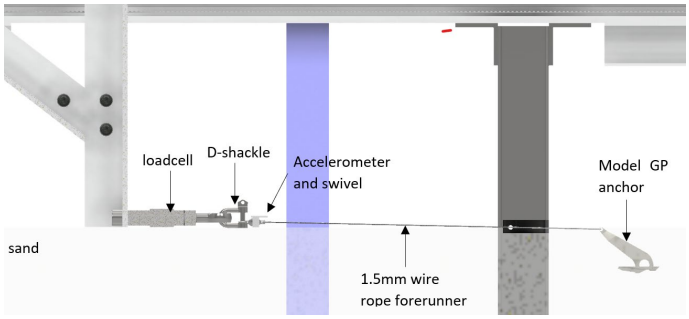

Figure 2. Schematic section view of anchor towing arrangement of centrifuge equipment for straight line pulls

Out-of-plane loading of the anchor required modifications of the original equipment as shown in Figure 3. A second motor (DOGA 319 hall) and winch were added to the actuator with a wire rope routed from the winch over two pulleys to the surface of the sand bed for attachment to the wire rope used in the straight pull of the anchor. Support for the lowermost pulley used to change the direction of the out-of-plane rigging was provided by a steel box section mounted in a fixed location to the base of the box and the underside of the actuator.

Since the out-of-plane towing position was fixed, the position of the anchor was varied to provide side-pulls at different angles. The lowermost pulley was a swivel type and a slot was cut in the box section to allow for side-pull angles from 20 to 90°. The side-pull tow force was measured by a loadcell mounted in-line in the wire rope system, between the upper and lower pulleys (Figure 3). This loadcell comprised a full Wheatstone-bridge arrangement of strain gauges and was calibrated to 2kN. Displacement of the anchor was again measured indirectly by counting pulses from the hall-effect sensors in the

motor which were calibrated to the number of turns of the winch.

Actuator control and data acquisition (at 250Hz) was achieved with a National Instruments 9047 CompactRIO. Video footage of the anchor was recorded for each test using GoPro cameras.

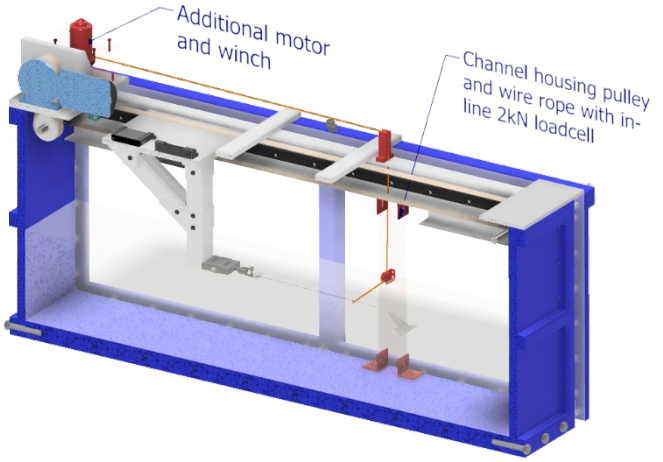

Figure 3. Half-view of centrifuge box and actuator with new equipment for side-pull tests coloured red

2.4 *Sand bed properties and preparation*

The dry HST95 sand used for all tests herein and in previous studies at the University of Dundee (e.g. Lauder et al. (2013), Bertalot and Brennan (2015), (Jeffrey et al., 2016, and Davidson et al., 2020) has been extensively characterised. HST95 is a fine-grained quarzitic sand with D_{10} and D_{50} particle sizes of 0.10 and 0.14mm respectively (Lauder et al., 2013). Relevant properties of HST95 are presented in Table 2.

Table 2. HST95 sand properties (Al-Defae, 2013, Lauder, 2010).

Property	Value
Effective particle size, D_{10} (mm)	0.09
Average particle size, D_{50} (mm)	0.14
Critical state friction angle, ϕ'_{crit} (°)	32
Angle of dilation* at D_r = 60%, ψ (°)	11.2
Peak friction angle* at D_r = 60%, ϕ'_{pk} (°)	41
Maximum dry density, ρ_{max} (kN/m^3)	17.58
Minimum dry density, ρ_{min} (kN/m^3)	14.59

*Inferred from best-fit peak strength relationship from direct shear tests for data at effective stresses between 50-200kPa and critical state friction angle, at 60% relative density (Al-Defae et al., 2013).

To control the density of the sand, a slot pluviation system was used. The slot pluviator consists of a tapered hopper with a slot, which can be varied in width. The rail-mounted hopper is moved back and forth at a constant speed and at 1.2m above the model container with a motor to "rain" sand into the box. The slot width was set to give relative densities of ~55 ±5% for the medium-dense sand bed. Such air-pluviation methods provide reliably uniform and consistent sand beds.

Consistent samples of loose sand are difficult to achieve with the air-pluviation method. Instead, the sand in the box was disturbed by thorough stirring. The large displacement of the sand caused by stirring creates a loose density of ~35% for all loose sand tests. Finally, a plastic scraper was run along the top of the box to create a flat and level surface.

2.5 *Model drag embedment anchor*

All tests used a 1/80th scaled version of a 12t Bruce GP drag embedment anchor created using 3D printing methods to ensure an accurate representation of the anchor geometry. To maintain a representative centre of gravity and projected section area, the shank and upper portion of the model were printed using stainless steel while the underside of the fluke was printed in ABS plastic. This approach also enabled a 3-axis accelerometer to be placed inside the fluke. The analogue MEMS accelerometer chip (ADXL377z) was glued to the underside of the fluke so that the x-axis and y-axis were aligned port/starboard and fore/aft respectively (Figure 5). Data from the accelerometer were used to calculate the pitch (p) and roll (r) of the anchor using equations 1 and 2.

$$p = \tan^{-1}\frac{y}{\sqrt{x^2+z^2}}/2\pi \times 360 \quad (1)$$

$$r = \tan^{-1}\frac{x}{\sqrt{y^2+z^2}}/2\pi \times 360 \quad (2)$$

Direct measurements of the depth of the anchor were not possible during the test, thus, to estimate the depth of the anchor, a second accelerometer was added to the forerunner/towline. Observations from preliminary tests showed that the forerunner was likely taut during the test, i.e. did not form a catenary shape. Assuming a straight forerunner and knowing the length (440mm) and pitch of the forerunner line via the accelerometer data it was possible to estimate, using simple trigonometry, the depth of the anchor padeye after the initial embedment of the anchor took place and the forerunner angle became steady.

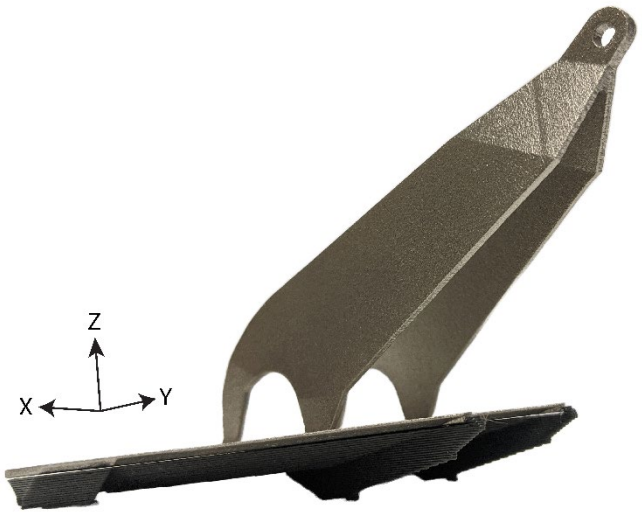

Figure 4. 1/80th scale model GP anchor. Shank and upper fluke 3D printed in metal (silvery colour) and lower fluke 3D printed in ABS plastic (grey).

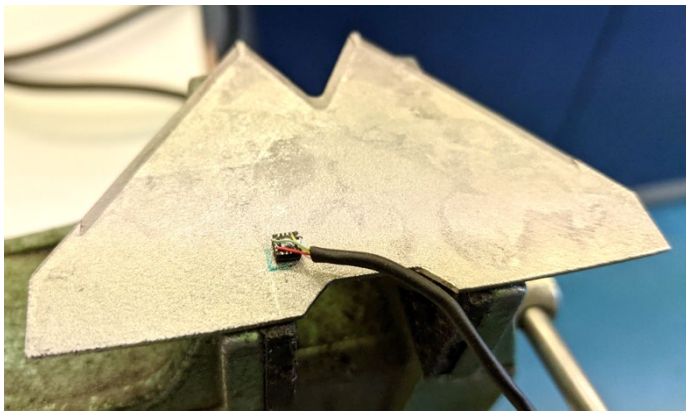

Figure 5. ADXL377 accelerometer MEMS chip mounted on underside of fluke

Subsequent development of more advanced instrumentation which utilises wireless communication has been developed by Sharif et al. (2023) to enable continuous depth measurements of the anchor derived from accelerometer and gyroscope sensors embedded within the anchor.

Both accelerometers were calibrated at 1g by aligning each axis parallel to earth's gravity and recording the maximum and minimum values to determine the calibration factors and baseline voltages (Robinson et al., 2019). The absolute g-level (a) recorded by the sensor is calculated by equation 3. Verification of the sensor calibration was provided by the calculated g values matching the g-force generated by the centrifuge.

$$|a| = \sqrt{x^2 + y^2 + z^2} \quad (3)$$

2.6 *Test Programme*

Details of the five tests conducted on the centrifuge are presented in Table 3 which provides information on the soil conditions, angle of loading and any pre-embedment of the anchor required to generate the 60% of UHC in the space available to drag the anchor before reaching the point where the side-pull test was conducted.

Table 3. Test programme details. S = straight, O = out of plane

Test name	Relative density (%)	Type	Out of plane pull angle (°)	Pre-embedded (m)
L	33.5	S	-	-
MD	55.3	S	-	-
MD-20	58.6	O	20	10
MD-30	53.1	O	30	-
MD-45	53.1	O	45	-

3 **Results and discussion**

3.1 *Introduction*

Data presented in this section from the tests show the load-displacement, depth, and attitude of the anchor. The two phases (pre-loading or "keying" to a percentage of UHC and subsequent side-pull) of the out-of-plane (OOP), or side-pull, tests are presented as a single sequence, where the force returns to zero at the end of the keying stage.

3.2 *Straight UHC pulls*

Figure 6 presents load-displacement, attitude (pitch and roll) and depth data for the straight pulls completed in loose and medium-dense sand to determine the ultimate holding capacity of the anchor.

The ultimate holding capacity (UHC) for the given sand density is defined in these tests as the maximum observed towing force, which is not necessarily coincident with steady state conditions.

The stiffness behaviour of the anchor in the initial 20m drag distance is very similar between all tests as shown by the similarity of the slope of the load-displacement curves in Figure 6a. From this data, it is apparent that the anchor did not reach a steady state condition in the loose test (L) since the load was observed to still be increasing at the end of the test (defined by the maximum allowable drag distance). It is therefore likely that the ultimate capacity of the GP anchor in the loose sand tested is greater than the maximum 811t measured at 50m drag distance.

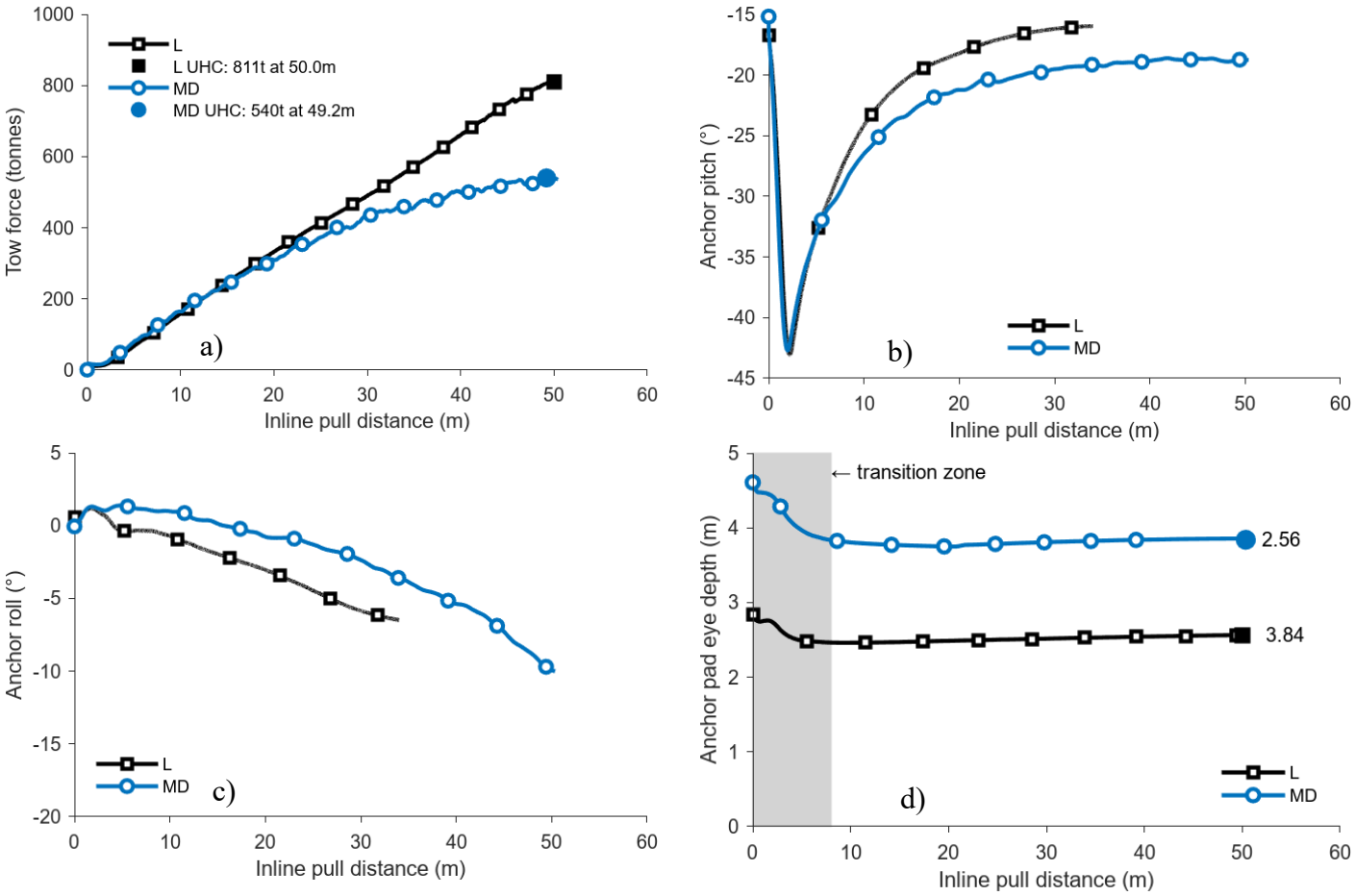

Figure 6. Straight pull data from tests L and MD in loose and medium-dense sand respectively: a)tow force, b) pitch, c) roll, d) padeye depth The ultimate holding capacity (UHC) is shown for each test by a solid symbol with values given in the legend. Note, the anchor accelerometer wiring broke in test L at 32 m displacement. Shaded area in d) indicates transition zone of data from initial reorientation of the forerunner accelerometer.

Although the accelerometer wiring was damaged at 32m drag distance in the loose test, it appears from the available data that the anchor pitch was beginning to plateau. From this observation it may be possible to say that the pitch of the anchor at steady state is density dependant, with a more horizontal fluke in looser relative densities of sand.

Ultimate holding capacities of the anchor determined from the maximum force of the straight pull centrifuge tests are 811 and 540 tonnes in loose (L) and medium-dense (MD) sand respectively. These UHC values were observed at 50 and 49.2m.

From the calculated anchor depth data, a clear difference in depth of the GP anchor was seen in the straight pull tests in the two different relative densities of sand (Figure 6d). The calculation method for determining padeye depth (section 2.5) requires a taut cable which is not guaranteed before about 8 m lateral displacement. This data is therefore shaded in Figure 6d, and may be considered indicative only. Beyond this distance, the depth of the padeye of the anchor can be seen to reach a relatively steady-state, with only minor changes in depth occurring to the end of the test. Considering the padeye depth in isolation would suggest that the pull force would be at a constant value when the padeye depth is constant in the uniform sand conditions. However, this is not the case as shown in Figure 6a where the force continues to increase with distance. This is likely explained by the continual decrease (becoming more horizontal) in pitch of the anchor (Figure 6b) equating to increased fluke depth and pull force.

3.3 *Out-of-plane centrifuge tests*

Three out of plane tests at three side-pull angles were conducted in medium-dense sand beds to examine the anchor performance when subject to lateral loads. Each side-pull was conducted after loading or "keying" the anchor to a target of 0.6UHC. Next, the forerunner was reconfigured to the side-pull arrangement and the anchor pulled ~6.4 –7.2m. An accelerometer on the side-pull towline was not possible and thus, no depth data are available from the side-pull tests other than from a manual measurement taken by probing into the sand with a thin rod after the test.

The centrifuge actuator operates on a displacement-controlled basis where a predetermined distance is entered and when reached the software stops the motor. This approach does not allow for specific

loads to be used as a control. Therefore, the drag distance required to reach the target load of 0.6UHC was determined from the load-displacement data of the straight pull tests and that distance was set as the target for the keying of the side-pull tests. The required position of the anchor in the 20° medium-dense side-pull tests meant pre-embedment of the anchor at 1g by pushing the model vertically into the sand was required. The anchor was then dragged to the target location for the side-pull test to finish the keying stage. Summary data in Table 4 shows target loads of 0.6UHC were achieved to within ±0.05 in all but one of the tests (0.47UHC for medium dense 20° test).

Out-of-plane pulls of the anchor were conducted at 20, 30 and 45° in medium-dense sand. The measured pull forces of the anchor in the keying stages of the medium-dense side-pull tests are consistent with the straight pull test (MD-S) as shown in Figure 7a.

A limited amount of anchor roll (<10°) occurred in these tests. The pitch and depth of the anchor are similar in all three side-pull tests (Figure 7c and d). Such rolling of drag embedment anchors is also reported from field and other model tests (e.g. (LeLievre and Tabatabaee, 1981, and Naval Civil Engineering Lab, 1981).

The attitude of the anchor was observed to change during the medium-dense lateral tests with notable increases in the pitch and roll of the anchor. However, in all three tests, this change in attitude occurs after a period of relatively steady pitch and roll for distances of 1.8, 0.7 and 1.5m for the 20, 30 and 45° side-pull angles respectively (Figure 7b and c).

Table 4. Summary of drag distances and loads from all centrifuge out-of-plane (OOP) tests. *pre-embedded at 10m equivalent drag distance

Test name	Relative density (%)	OOP side-pull angle (°)	Out of plane pull angle (°)	Keying stage			Out of plane pull		
				Total Drag distance (m)	Force (tonnes)	% UHC	Total drag distance (m)	Max force (tonnes)	% UHC
MD-20	58.6	O	20	14.8*	256	0.47	7.6	326	0.60
MD-30	53.1	O	30	21.8	356	0.65	7.4	343	0.66
MD-45	53.1	O	45	17.6	295	0.55	6.9	288	0.53

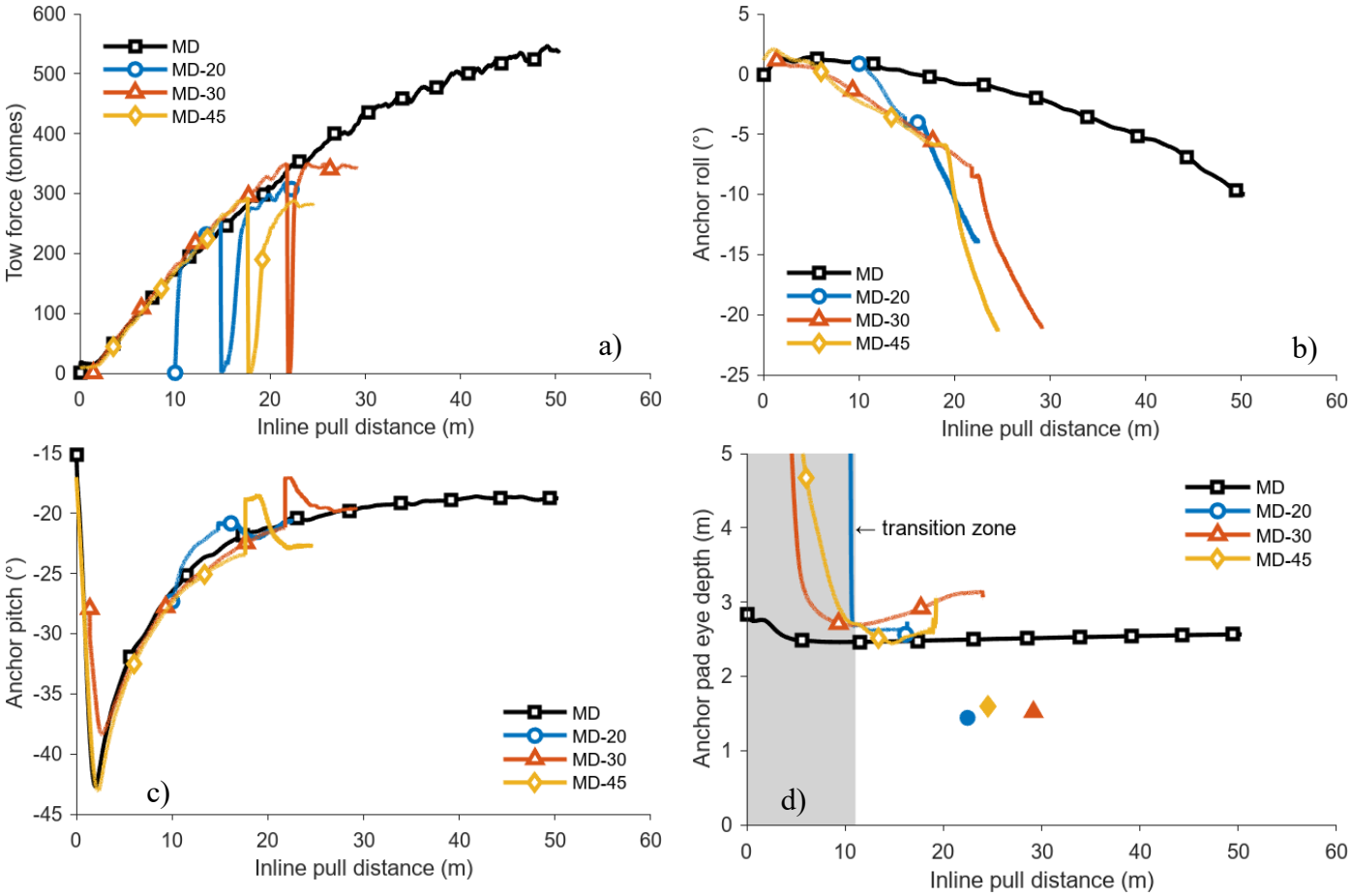

Figure 7. Data for out-of-plane tests in medium-dense sand with side-pull angles of 20, 30 and 45° (tests MD-20, MD-30, MD-45 respectively). Straight pull test MD is shown for reference. a) tow force, b) roll, c) pitch, d) padeye depth. The final depth, measured manually by excavating sand around the anchor, is shown by a solid symbol

This behaviour is attributed to yawing of the anchor around the vertical z-axis in adjustment to the new direction of pull. This is followed by a transition period where the anchor reaches a new steady pitch angle, similar to that in the straight pull (Figure 7c), and continues to roll, but at a more aggressive rate than in the keying stage of the tests (Figure 7b). The depth of the anchor was again measured at the end of each side-pull by uncovering the anchor and measuring the depth of the padeye below the sand surface. At all three side-pull angles, the anchor finished in a shallower position than at the beginning of the side-pull test (Figure 7d).

The pull force data in shows that in the medium-dense sand, the anchor regained all or most of the pull force seen in the straight pull reference test (MD-S), while being pulled laterally. In the side-pull tests at 20 and 30°, the anchor was able to return to the backbone curve of the straight pull test, achieving 60% UHC before the test stopped. Note that the 30° pull appears to peak at this point, and the 20° pull may have additional capacity although a slightly lower keying load was achieved in this test. The peak tow force observed in the 45° angle pull was not able to regain the backbone curve, peaking at 81% of the straight pull test (53% UHC) after the same total drag distance. From this data it may be suggested that the GP anchor has similar performance at side-pull angles up to 20° as for an in-plane (0°) pulls in these tests. However, any changes in loading direction of the anchor may require additional displacement of the anchor and the effects of such anchor movement should be considered in the design.

4 Conclusions

This paper has demonstrated the use of centrifuge tests for assessment of the holding capacity and behaviour of a drag embedment anchor under straight and out-of-plane loading conditions in loose and medium-dense soil.

Straight pull tests of the anchor provided data on the holding capacity up to a drag distance of 50m. Side-pull tests at angles of 20, 30 and 45° were conducted in medium-dense sand after pulling the anchor to 60% of the maximum load from the straight pull tests. The results indicate that the angle at which the side loading is applied is likely a controlling factor on the holding capacity of the anchor under such side-loading conditions.

Under the test conditions, the anchor was found to achieve similar holding capacities under a 20° side load to those observed in the straight pull reference test. At greater side-pull angles (e.g. 30 and 45°) in medium-dense sand, the holding capacities were lower than measured in the straight pull test.

These findings highlight the importance of the loading angle on the performance of the anchor and demonstrate that care must be exercised when designing systems which could potentially induce side-loading of the anchors.

Further work is planned to further investigate the side-loading behaviour of the anchor embedded in different soil conditions and also under inclined loading conditions. Newly developed wireless instrumentation is recommended to provide higher quality anchor depth information for more detailed analysis of the anchor behaviour under variable loading conditions.

5 References

AL-DEFAE, A. H., CAUCIS, K. & KNAPPETT, J. A. 2013. Aftershocks and the whole-life seismic performance of granular slopes. *Géotechnique,* 63**,** 1230-1244.

AL-DEFAE, A. H. H. 2013. *Seismic performance of pile-reinforced slopes.* PhD PhD, University of Dundee.

BERTALOT, D. & BRENNAN, A. J. 2015. Influence of initial stress distribution on liquefaction-induced settlement of shallow foundations. *Géotechnique,* 65**,** 418-428.

DAVIDSON, C., BROWN, M. J., CERFONTAINE, B., AL-BAGHDADI, T., KNAPPETT, J. A., BRENNAN, A. J., AUGARDE, C., COOMBS, W., WANG, L., BLAKE, A., RICHARDS, D. & BALL, J. 2020. Physical modelling to demonstrate the feasibility of screw piles for offshore jacket-supported wind energy structures. *Géotechnique,* 72**,** 108-126.

JEFFREY, J. R., BROWN, M. J., KNAPPETT, J. A., BALL, J. D. & CAUCIS, K. 2016. CHD pile performance: part I – physical modelling. *Proceedings of the Institution of Civil Engineers - Geotechnical Engineering,* 169**,** 421 – 435.

LAUDER, K. 2010. *The performance of pipeline ploughs.* PhD PhD, University of Dundee.

LAUDER, K. D., BROWN, M. J., BRANSBY, M. F. & BOYES, S. 2013. The influence of incorporating a forecutter on the performance of offshore pipeline ploughs. *Applied Ocean Research,* 39**,** 121 – 130.

LELIEVRE, B. & TABATABAEE, J. 1981. The performance of marine anchors with planar

flukes in sand. *Canadian Geotechnical Journal,* 18**,** 520-534.
UIR WOOD, D. 2014. *Geotechnical Modelling,* London, UK, Spon Press.
NAVAL CIVIL ENGINEERING LAB 1981. Drag Embedment Anchor Tests in Sand and Mud. Port Hueneme, California, USA: Naval Civil Engineering Lab.
ROBINSON, S., BROWN, M. J., MATSUI, H., BRENNAN, A., AUGARDE, C., COOMBS, W. & CORTIS, M. 2019. Centrifuge testing to verify scaling of offshore pipeline ploughs. *International Journal of Physical Modelling in Geotechnics,* 19**,** 305-317.
SHARIF, Y. U., BROWN, M. J., COOMBS, W., AUGARDE, C., BIRD, R., CARTER, G., MACDONALD, C. & JOHNSON, K. R. 2023. Characterisation of anchor penetration behaviour for Cable burial risk assessment in sand. *9th International SUT OSIG Conference "Innovative Geotechnologies for Energy Transition"*. London, UK.